Available online at www.sciencedirect.com
SCIENCE DIRECT®
Journal of Magnetic Resonance 162 (2003) 402–416
JMR Journal of Magnetic Resonance
www.elsevier.com/locate/jmr

SCAM-STMAS: satellite-transition MAS NMR of quadrupolar nuclei with self-compensation for magic-angle misset

Sharon E. Ashbrook and Stephen Wimperis*

School of Chemistry, University of Exeter, Stocker Road, Exeter EX4 4QD, UK

Received 25 October 2002; revised 16 January 2003

Abstract

Several methods are available for the acquisition of high-resolution solid-state NMR spectra of quadrupolar nuclei with half-integer spin quantum number. Satellite-transition MAS (STMAS) offers an approach that employs only conventional MAS hardware and can yield substantial signal enhancements over the widely used multiple-quantum MAS (MQMAS) experiment. However, the presence of the first-order quadrupolar interaction in the satellite transitions imposes the requirement of a high degree of accuracy in the setting of the magic angle on the NMR probehead. The first-order quadrupolar interaction is only fully removed if the sample spinning angle, χ, equals $\cos^{-1}(1/\sqrt{3})$ exactly and rotor synchronization is performed. The required level of accuracy is difficult to achieve experimentally, particularly when the quadrupolar interaction is large. If the magic angle is not set correctly, the first-order splitting is reintroduced and the spectral resolution is severely compromised. Recently, we have demonstrated a novel STMAS method (SCAM-STMAS) that is self-compensated for angle missets of up to $\pm 1^\circ$ via coherence transfer between the two different satellite transitions $\mathrm{ST}^+(m_I = +3/2 \leftrightarrow +1/2)$ and $\mathrm{ST}^-(m_I = -1/2 \leftrightarrow -3/2)$ midway through the t_1 period. In this work we describe in more detail the implementation of SCAM-STMAS and demonstrate its wider utility through ^{23}Na ($I = 3/2$), ^{87}Rb ($I = 3/2$), ^{27}Al ($I = 5/2$), and ^{59}Co ($I = 7/2$) NMR. We discuss linewidths in SCAM-STMAS and the limits over which angle-misset compensation is achieved and we demonstrate that SCAM-STMAS is more tolerant of temporary spinning rate fluctuations than STMAS, resulting in less "t_1 noise" in the two-dimensional spectrum. In addition, alternative correlation experiments, for example involving the use of double-quantum coherences, that similarly display self-compensation for angle misset are investigated. The use of SCAM-STMAS is also considered in systems where other high-order interactions, such as third-order quadrupolar effects or second-order quadrupole–CSA cross-terms, are present. Finally, we show that the sensitivity of the experiment can be improved through the use of amplitude-modulated pulses.

1. Introduction

The acquisition of high-resolution solid-state NMR spectra of half-integer quadrupolar nuclei may be achieved using the recently developed satellite-transition (ST) magic-angle spinning (MAS) NMR experiment [1,2]. This technique is conceptually similar to the widely used multiple-quantum (MQ) MAS method [3], with both experiments involving two-dimensional correlation under MAS conditions. In MQMAS, this correlation is between a multiple-quantum transition (e.g., $m_I = +3/2 \leftrightarrow -3/2$) and the central transition ($m_I = +1/2 \leftrightarrow -1/2$), while in STMAS the correlation involves (single-quantum) satellite transitions (e.g., $m_I = \pm 3/2 \leftrightarrow \pm 1/2$) and the central transition (CT). The second-order quadrupolar broadening [4,5] of the transitions involved in each experiment differ only by a simple scaling factor, allowing this interaction to be refocussed and a high-resolution or "isotropic" spectrum to be obtained.

Despite recent advances [6–9], the low efficiency of the excitation and conversion of multiple-quantum coherences, particularly those of higher coherence order, remains a severe limitation of MQMAS [10,11]. In contrast, the STMAS experiment involves purely single-quantum coherences, thus potentially offering a significant sensitivity advantage over MQMAS [1,2], experimentally often found to be a factor of 3 or more [12,13].

* Corresponding author. Fax: +44-1392-263434.
E-mail address: s.wimperis@exeter.ac.uk (S. Wimperis).

1090-7807/03/$ - see front matter © 2003 Elsevier Science (USA). All rights reserved.
doi:10.1016/S1090-7807(03)00016-8

Furthermore, the STMAS signal intensity is predicted to remain largely invariant as the spinning rate is increased [13], whereas the MQMAS signal intensity becomes significantly reduced at high MAS rates [14]. In STMAS, however, the presence of the large first-order quadrupolar interaction in the satellite transitions necessitates both a very high degree of accuracy in the setting of the magic angle on the NMR probehead (often better than $\pm 0.004°$) [1,13] and a stable MAS rate to allow rotor-synchronized t_1 acquisition [1,2]. These technically demanding requirements have proved the major restrictions on the practical implementation of STMAS.

Recently, we have introduced a novel STMAS experiment (SCAM-STMAS) that is self-compensated for angle missets of up to $\pm 1°$ [15]. When the angle between the sample rotation axis and the magnetic field B_0 is not set accurately to the magic angle ($\cos^{-1}(1/\sqrt{3}) = 54.736°$) the first-order quadrupolar interaction is reintroduced into the satellite transitions, thereby significantly reducing the spectral resolution. The two satellite transitions $\mathrm{ST}^+(m_I = +3/2 \leftrightarrow +1/2)$ and $\mathrm{ST}^-(m_I = -1/2 \leftrightarrow -3/2)$ have first-order quadrupolar interactions that are equal in magnitude but of opposite sign. Therefore, if the t_1 period of an STMAS experiment is split into two halves to allow evolution of ST^+ coherences followed by evolution of ST^- coherences (and vice versa), the first-order quadrupolar interaction will be refocussed, once again yielding a high-resolution spectrum. The aim of the SCAM-STMAS technique, therefore, is to allow STMAS to be implemented in cases where (i) for instrumental reasons, the magic angle cannot be set with the accuracy required by the original version of the technique and (ii) the quadrupolar interaction is very large and, even with ideal, state-of-the-art instrumentation, it is difficult to set the magic angle with sufficient accuracy.

In this work we describe in more detail the implementation and uses of SCAM-STMAS, using ^{23}Na ($I = 3/2$), ^{87}Rb ($I = 3/2$), ^{27}Al ($I = 5/2$), and ^{59}Co ($I = 7/2$) NMR as examples. The possible limits of angle misset over which compensation is achieved are considered. The SCAM-STMAS experiment is shown to display greater tolerance to small fluctuations in spinning rate than STMAS, resulting in much less "t_1 noise" in the two-dimensional spectrum. For nuclei with spin quantum number $I > 3/2$, SCAM-STMAS experiments that refocus $m_I = \pm 5/2 \leftrightarrow \pm 3/2$, or $\mathrm{ST}_2^{\pm}$, satellite transitions are possible and these are demonstrated using ^{27}Al NMR. In addition, alternative refocussing experiments involving double-quantum coherences ($m_I = \pm 3/2 \leftrightarrow \mp 1/2$) are described. The use of SCAM-STMAS is also discussed in systems where other high-order effects, such as third-order quadrupolar interactions or second-order quadrupolar–CSA cross-terms are present. Finally, it is shown that the sensitivity of SCAM-STMAS experiments may be increased through the use of amplitude-modulated, or FAM-type [7], pulses.

2. General experimental details

Experiments were performed using a Bruker Avance 400 spectrometer equipped with a widebore 9.4 T magnet, operating at a Larmor frequency, ν_0, of 105.8 MHz for ^{23}Na, 104.3 MHz for ^{27}Al, 94.5 MHz for ^{59}Co, and 130.9 MHz for ^{87}Rb. A conventional Bruker MAS probe was used, with powdered solids packed inside 2.5-mm rotors and inserted/ejected pneumatically. Spinning rates, ν_R, were between 10 and 30 kHz. Radiofrequency field strengths, $\nu_1 = |\gamma B_1|/2\pi$, were between 130 and 180 kHz. When required, highly accurate setting of the magic angle was achieved by maximising the height of the ST → CT shifted-echo ^{87}Rb signal in a one-dimensional STMAS experiment [12,13] and confirmed by running a two-dimensional STMAS spectrum of $RbNO_3$. In the off-angle STMAS and SCAM-STMAS experiments described here, the misset of the magic angle was estimated by comparison with simulated spectra: note, however, that there would be no need for this in routine use of SCAM-STMAS. Other experimental details are given in the figure captions.

Andalusite (South Africa) was obtained from a private mineral collection. All other materials were purchased commercially and used without further purification.

3. Background to STMAS

In a reference frame rotating at ν_0, the frequency of a $m_I = \pm(q-1) \leftrightarrow \pm q$ single-quantum transition (with $q = 1/2, 3/2, \ldots, I$) can be written for a rapidly spinning sample as the sum of first- and second-order terms

$$\nu_{\pm(q-1)\leftrightarrow\pm q} = \nu^{(1)}_{\pm(q-1)\leftrightarrow\pm q} + \nu^{(2)}_{\pm(q-1)\leftrightarrow\pm q}. \quad (1)$$

If, for simplicity, axial symmetry of the quadrupole tensor is assumed, i.e., $\eta = 0$, the contributions from the first- and second-order quadrupolar interactions are given by

$$\nu^{(1)}_{\pm(q-1)\leftrightarrow\pm q} = \pm(2q-1)\nu_Q^{\mathrm{PAS}} d^2_{0,0}(\chi) d^2_{0,0}(\beta), \quad (2)$$

$$\nu^{(2)}_{\pm(q-1)\leftrightarrow\pm q} = \frac{(\nu_Q^{\mathrm{PAS}})^2}{\nu_0}\Big\{\mathrm{A}^0(I,q) + \mathrm{A}^2(I,q) d^2_{0,0}(\chi) d^2_{0,0}(\beta) + \mathrm{A}^4(I,q) d^4_{0,0}(\chi) d^4_{0,0}(\beta)\Big\}, \quad (3)$$

respectively. Here, χ is the angle between the sample rotation axis and the external magnetic field B_0, β is the Euler angle describing the orientation of the quadrupole tensor with respect to the spinning axis, and the $d^l_{m',m}(\theta)$ are reduced Wigner rotation matrix elements of rank l

Table 1
Spin- and transition-dependent coefficients, $A^l(I,q)$, for $m_I = \pm(q-1) \leftrightarrow \pm q$ single-quantum transitions

	$A^0(I,q)$	$A^2(I,q)$	$A^4(I,q)$
$I = 3/2$			
$q = 1/2$ (CT)	−2/5	−8/7	54/35
$q = 3/2$ (ST)	4/5	20/35	−48/35
$I = 5/2$			
$q = 1/2$ (CT)	−16/15	−64/21	144/35
$q = 3/2$ (ST_1)	2/15	−20/15	6/5
$q = 5/2$ (ST_2)	56/15	80/21	−264/35
$I = 7/2$			
$q = 1/2$ (CT)	−30/15	−120/21	270/35
$q = 3/2$ (ST_1)	−12/15	−140/35	168/35
$q = 5/2$ (ST_2)	42/15	8/7	−138/35
$q = 7/2$ (ST_3)	132/15	340/35	−648/35
$I = 9/2$			
$q = 1/2$ (CT)	−48/15	−192/21	432/35
$q = 3/2$ (ST_1)	−30/15	−156/21	330/35
$q = 5/2$ (ST_2)	24/15	−48/21	24/35
$q = 7/2$ (ST_3)	114/15	132/21	−486/35
$q = 9/2$ (ST_4)	240/15	384/21	−1200/35

[16]. The quadrupolar frequency parameter, ν_Q^{PAS}, is given by $3C_Q/4I(2I-1)$, where $C_Q = e^2qQ/h$. The spin- and transition-dependent coefficients, $A^l(I,q)$, can be calculated using perturbation theory and are given in Table 1. Note that for the central transition, where $q = 1/2$, the first-order quadrupolar interaction, proportional to $(2q-1)$, is always zero, in contrast to the satellite ($q = 3/2, 5/2, \ldots, I$) transitions.

If sample rotation is performed at precisely the magic angle ($\chi = \cos^{-1}(1/\sqrt{3})$), the second-rank reduced rotation matrix elements $d^2_{0,0}(\chi)$ in Eqs. (2) and (3) are zero and the first-order quadrupolar interaction is removed from all transitions. However, the second-order quadrupolar interaction is not fully removed as the fourth-rank anisotropic term in Eq. (3), proportional to $d^4_{0,0}(\chi)$, remains [4]. All transitions now comprise an isotropic shift, $A^0(I,q)\ (\nu_Q^{PAS})^2/\nu_0$, and, in a powdered solid, an anisotropic fourth-rank quadrupolar broadening, proportional to $A^4(I,q)\ (\nu_Q^{PAS})^2/\nu_0$. Thus, under MAS, the quadrupolar broadenings of the central and satellite transitions differ by a simple factor.

The pulse sequence for a shifted-echo STMAS experiment is shown in Fig. 1a [12,13]. This technique correlates satellite transitions in the (rotor-synchronized) t_1 period with the central transition in the t_2 period of a two-dimensional experiment, a correlation that we denote ST → CT. A fixed (rotor-synchronized) τ interval is present in order to acquire a whole-echo signal and obtain two-dimensional lineshapes which are in pure absorption [17,18]. When $t_2/t_1 = A^4(I,q \neq 1/2)/A^4(I,1/2)$ the fourth-rank anisotropic broadening is refocussed while the isotropic shifts are retained. A complex (not hypercomplex!) Fourier

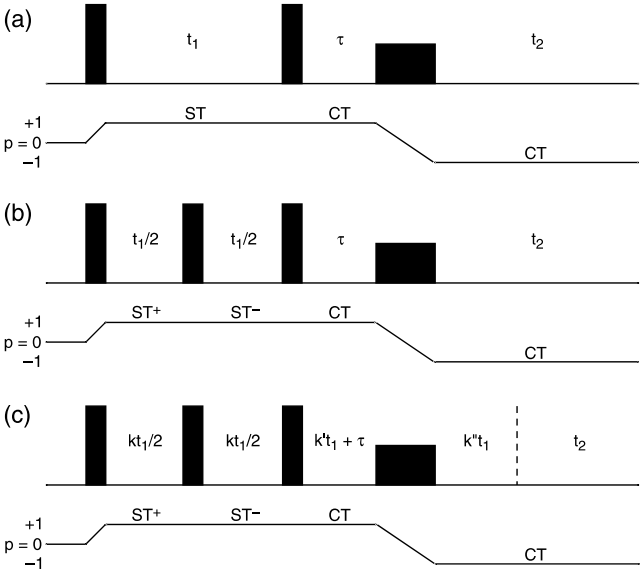

Fig. 1. Pulse sequence and coherence transfer pathway for (a) three-pulse shifted-echo STMAS experiment, (b) STMAS experiment with self-compensation for magic-angle misset (SCAM), and (c) split-t_1 SCAM-STMAS experiment. In (c), k, k', and k'' are chosen to refocus the second-order quadrupolar broadening at the end of the t_1 period ($k = (1 + |R(I,q)|)^{-1}$ and $k + k' + k'' = 1$, with $k' = 0$ for $R(I,q) > 0$ and $k'' = 0$ for $R(I,q) < 0$). In (a), a 32-step phase cycle can be used to select the desired coherence pathways: first pulse, 0°; second pulse, 0° 45° 90° 135° 180° 225° 270° 315°; third pulse, 8(0°) 8(90°) 8(180°) 8(270°); receiver, 8(0°) 8(180°). In (b), a 100-step phase cycle can be used: first pulse, 0°; second pulse, 0°, 72°, 144°, 216°, 288°; third pulse, 5(0°), 5(72°), 5(144°), 5(216°), 5(288°); fourth pulse, 25(0°), 25(90°), 25(180°), 25(270°); receiver, 25(0°), 25(180°).

transformation yields a two-dimensional spectrum that consists of a series of ridge-like lineshapes corresponding to the crystallographically distinct sites. The ridges lie along a gradient equal to the ratio of the fourth-rank broadenings, $A^4(I,q \neq 1/2)/A^4(I,1/2)$, termed the STMAS ratio, $R(I,q)$ [1,2,13]. A high-resolution one-dimensional spectrum is obtained from a projection orthogonal to this gradient. Fig. 2a displays a spin $I = 3/2$ STMAS spectrum simulated with $C_Q = 2$ MHz, $\eta = 0$, $\nu_0 = 100$ MHz and $\chi = 54.736°$ (the magic angle). The spectrum is shown so that the STMAS ridge appears parallel to the F_2 axis, as would be obtained after an appropriate shearing transformation [19]. The high-resolution or isotropic spectrum, now obtained from a projection onto the F_1 axis, consists of a single narrow resonance.

If the magic angle is misset, $d^2_{0,0}(\chi)$ is no longer zero and a first-order quadrupolar interaction is reintroduced into the satellite transitions [1,2] but not, as previously described, into the central transition. The perturbations of the two $q = 3/2$ satellite transitions are equal in magnitude but opposite in sign, resulting in a splitting, equal to $4\nu_Q^{PAS} d^2_{0,0}(\chi) d^2_{0,0}(\beta)$ if $\eta = 0$, in the F_1 dimension of the STMAS spectrum. This can be seen in Fig. 2b, where the sheared spectrum is simulated with

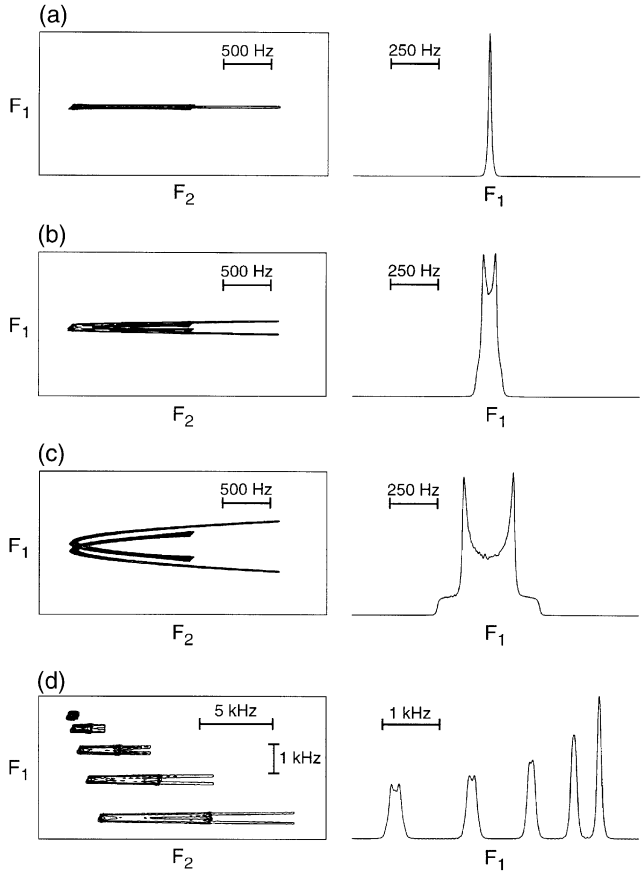

Fig. 2. Simulated two-dimensional $I = 3/2$ STMAS spectra and isotropic projections showing effects of spinning angle (χ) misset. (a–c) Single crystallographic site, with (a) $\chi = 54.736°$ (the magic angle), (b) 54.741°, and (c) 54.756°. Other parameters: $C_Q = 2$ MHz, $\eta = 0$, and $\nu_0 = 100$ MHz. (d) Five distinct sites with $C_Q = 1$, 2, 3, 4, and 5 MHz and $\chi = 54.741°$. Other parameters: $\eta = 0$, $\nu_0 = 100$ MHz. In each case the spectra are presented as if a shearing transformation has been used to yield the isotropic projection in the F_1 dimension.

$\chi = 54.741°$. The F_1 projection is no longer truly isotropic but contains a "Pake doublet" powder pattern, consistent with the reintroduction of a first-order quadrupolar interaction. The spectrum in Fig. 2c, simulated with $\chi = 54.756°$, shows a much greater effect with a significantly larger doublet splitting in the F_1 dimension. In contrast, the second-order quadrupolar shifts in both F_1 and F_2 frequency dimensions appear essentially unaffected by the angle misset as this interaction is proportional, not to ν_Q^{PAS} as for a first-order quadrupolar interaction, but to $(\nu_Q^{\mathrm{PAS}})^2/\nu_0$, which is typically one or two orders of magnitude smaller.

The unwanted effects of magic-angle misset become increasingly important when the quadrupolar interaction is large, owing to the dependence of the reintroduced first-order quadrupolar interaction upon ν_Q^{PAS}. Fig. 2d shows an $I = 3/2$ STMAS spectrum simulated for distinct nuclei with C_Q values of 1, 2, 3, 4 and 5 MHz, respectively. Other simulation parameters include $\eta = 0, \nu_0 = 100$ MHz and $\chi = 54.741°$. Five ridge lineshapes are observed and each displays a doublet splitting in the so-called isotropic projection. The splitting increases with increasing C_Q, resulting in a significant decrease in peak height.

4. Self-compensation for angle misset

Fig. 1b shows a pulse sequence for a STMAS experiment that is self-compensated for angle misset (SCAM-STMAS) [15]. Comparison with the conventional STMAS sequence in Fig. 1a shows that the t_1 period of the experiment is now split into two parts of equal duration by a pulse that induces coherence transfer between the ST^+ ($m_I = +3/2 \leftrightarrow +1/2$) and ST^- ($m_I = -1/2 \leftrightarrow -3/2$) transitions. Note that the $t_1/2$ periods must now be rotor synchronized, thereby halving the maximum F_1 spectral width, and that the $\mathrm{ST}^{\pm} \rightarrow \mathrm{ST}^{\mp}$, or SCAM, pulse must be phase-cycled so as to conserve the sign of the coherence order, p, thereby avoiding premature refocussing of the second-order shift. As the ST^+ and ST^- transitions possess first-order quadrupolar shifts that differ only in sign, this interaction can be refocussed allowing a high-resolution spectrum to once again be obtained.

Fig. 3 compares ^{23}Na STMAS and SCAM-STMAS NMR spectra of sodium oxalate ($Na_2C_2O_4$) in both the absence and presence of a misset of the spinning angle. Fig. 3a shows a two-dimensional ^{23}Na STMAS spectrum of $Na_2C_2O_4$ recorded with an accurate magic-angle setting. In addition to the peak resulting from $\mathrm{ST} \rightarrow \mathrm{CT}$ transfer lying along $R(3/2, 3/2) = -8/9$, there is a peak resulting from $\mathrm{CT} \rightarrow \mathrm{CT}$ transfer lying along the autocorrelation diagonal (+1) [1,12]. This peak is a characteristic feature of experimental STMAS spectra as, owing to its purely single-quantum nature, it cannot be removed by phase cycling. Different approaches for its removal have met with limited success, often at the expense of signal intensity [1,2,12,13,20]. When a significant magic-angle misset is present, estimated to be $\pm 0.07°$, the $\mathrm{ST} \rightarrow \mathrm{CT}$ peak displays a considerable δ_1 splitting, as shown in Fig. 3b. As expected, the $\mathrm{CT} \rightarrow \mathrm{CT}$ peak is unaffected.

Fig. 3c shows a two-dimensional ^{23}Na SCAM-STMAS spectrum of $Na_2C_2O_4$ recorded with an accurately set magic angle. The spectrum is similar to that in Fig. 3a except that an additional ridge is observed midway between the two ridges in the STMAS spectrum [15]. This is a consequence of the additional pulse in the SCAM-STMAS experiment which results in an increased number of possible single-quantum correlations. The peak resulting from $\mathrm{CT} \rightarrow \mathrm{CT} \rightarrow \mathrm{CT}$ transfer appears along the autocorrelation diagonal while $\mathrm{ST}^{\pm} \rightarrow \mathrm{ST}^{\mp} \rightarrow \mathrm{CT}$ and $\mathrm{ST}^{\pm} \rightarrow \mathrm{ST}^{\pm} \rightarrow \mathrm{CT}$ transfers yield the peak along −8/9. However, $\mathrm{ST}^{\pm} \rightarrow \mathrm{CT} \rightarrow \mathrm{CT}$ and $\mathrm{CT} \rightarrow \mathrm{ST}^{\pm} \rightarrow \mathrm{CT}$ transfers are also possible and

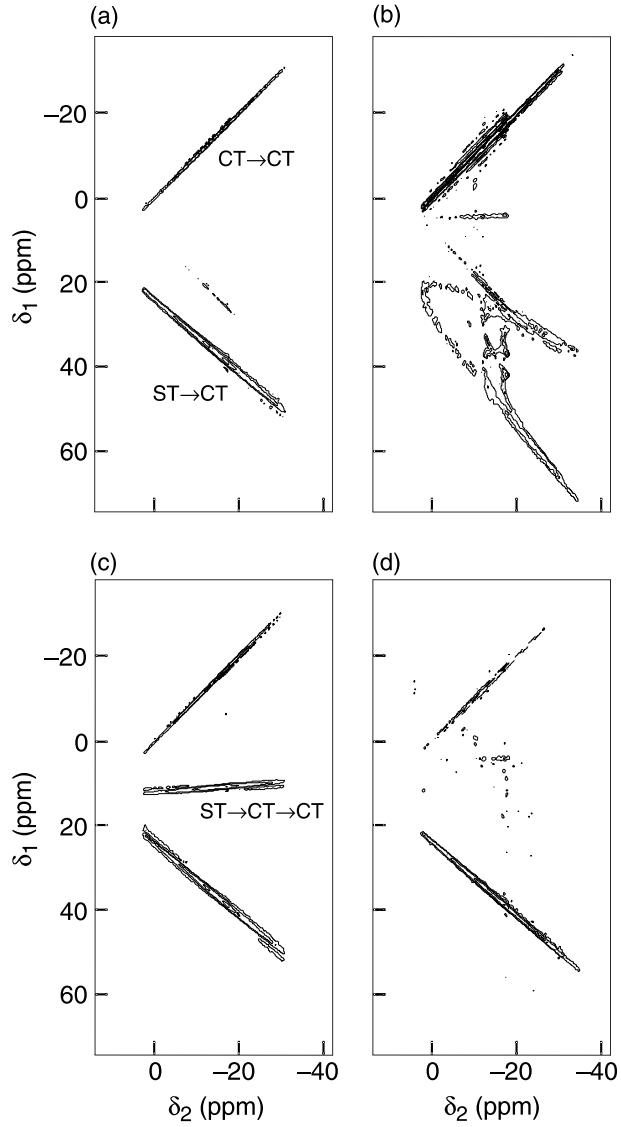

Fig. 3. ^{23}Na STMAS and SCAM-STMAS NMR of sodium oxalate, $Na_2C_2O_4$. (a,b) STMAS spectra recorded with the pulse sequence in Fig. 1a and (c,d) SCAM-STMAS spectra, recorded with the pulse sequence in Fig. 1b. In (a,c) the magic angle was set as accurately as possible, while in (b,d) the magic angle was misset by ~0.07°. In (a) 32, (b) 96, and (c,d) 200 transients were averaged with a recycle interval of 2.0 s for each of 128 t_1 increments of 66.6 μs. The MAS rate was 30 kHz. All ppm scales are referenced to 1.0 M NaCl (aq). Contour levels are shown at 10, 20, 40, and 80% of the maximum intensity.

appear midway between the former peaks with a gradient of $(+1 - 8/9)/2 = +1/18$. When the magic angle is set accurately all these peaks appear with significant intensity. In contrast, Fig. 3d shows the SCAM-STMAS spectrum recorded with an angle misset of ~0.07°. The $ST^{\pm} \rightarrow ST^{\pm} \rightarrow CT$, $ST^{\pm} \rightarrow CT \rightarrow CT$, and $CT \rightarrow ST^{\pm} \rightarrow CT$ peaks are now split by the first-order quadrupolar interaction and are almost unobservable. However, $ST^{\pm} \rightarrow ST^{\mp} \rightarrow CT$ transfer refocuses the first-order quadrupole interaction and results in a sharp ridge along a gradient of −8/9, allowing the acquisition of a high-resolution spectrum.

As with all pulses in MQMAS and STMAS, the parameters of the SCAM pulse should be carefully selected for optimum performance. The radiofrequency field strength should be as high as possible (as for the first and third pulses in Fig. 1b), while the pulse duration can often be optimised in a one-dimensional set-up experiment (performed off angle!), in a manner similar to that used for STMAS [13]. Frequently, we find that the optimum durations of the two "hard" STMAS pulses are both close to $(4\nu_1)^{-1}$ (e.g., ~1.5 μs if $\nu_1 \sim 150$ kHz), while a typical SCAM pulse is perhaps ~10% longer. Empirically, we have also found that the intensity of the peaks resulting from unwanted coherence changes, such as $ST^{\pm} \rightarrow CT \rightarrow CT$, may be reduced significantly by a judicious choice of the duration of the SCAM pulse.

Fig. 4a shows an ^{27}Al STMAS NMR spectrum of aluminium acetylacetonate ($Al(acac)_3$), recorded with the pulse sequence in Fig. 1a. As ^{27}Al has spin quantum number $I = 5/2$, two different satellite transitions are present: $q = 3/2$ (ST_1) with $m_I = \pm 3/2 \leftrightarrow \pm 1/2$ and $q = 5/2$ (ST_2) with $m_I = \pm 5/2 \leftrightarrow \pm 3/2$. Three ridges are present in the spectrum, therefore: $CT \rightarrow CT$ along +1, $ST_1 \rightarrow CT$ along $R(5/2, 3/2) = +7/24$, and $ST_2 \rightarrow CT$ along $R(5/2, 5/2) = -11/6$ [13]. The intensity of the $ST_2 \rightarrow CT$ peak is considerably lower than that of the $ST_1 \rightarrow CT$ peak mainly owing to the reduced efficiency of the coherence transfer processes [13]. Fig. 4b shows the STMAS spectrum recorded with an angle misset of ~0.09°. A significant first-order splitting is introduced into the STMAS peaks, resulting in a loss of resolution and a significant decrease in peak height. Eq. (2) predicts that the first-order splitting of the $q = 5/2$ or ST_2 satellite transitions will be larger than that of the $q = 3/2$ or ST_1 satellite transitions by a factor of two. In Fig. 4b, the $ST_2 \rightarrow CT$ peak is no longer observable at the contour levels shown. The $CT \rightarrow CT$ peak remains unaffected by the angle misset.

An ^{27}Al SCAM-STMAS spectrum, recorded using the pulse sequence in Fig. 1b with an accurately set magic angle, is shown in Fig. 4c. As was observed previously, an additional ridge is present in this spectrum, lying along $(+1 + 7/24)/2 = +31/48$, midway between the autocorrelation diagonal and the $q = 3/2$ STMAS ridge. This results from $ST_1^{\pm} \rightarrow CT \rightarrow CT$ and $CT \rightarrow ST_1^{\pm} \rightarrow CT$ coherence transfers. Other additional ridges are also present, resulting from correlations involving the $q = 5/2$ satellite transitions. Fig. 4d shows the ^{27}Al SCAM-STMAS spectrum recorded with an angle misset of ~0.09°. The unwanted ridges now experience a large first-order quadrupolar interaction and are barely observable. The $ST_1^{\pm} \rightarrow ST_1^{\mp} \rightarrow CT$ peak, however, consists of a intense narrow ridge allowing the high-resolution spectrum to be obtained.

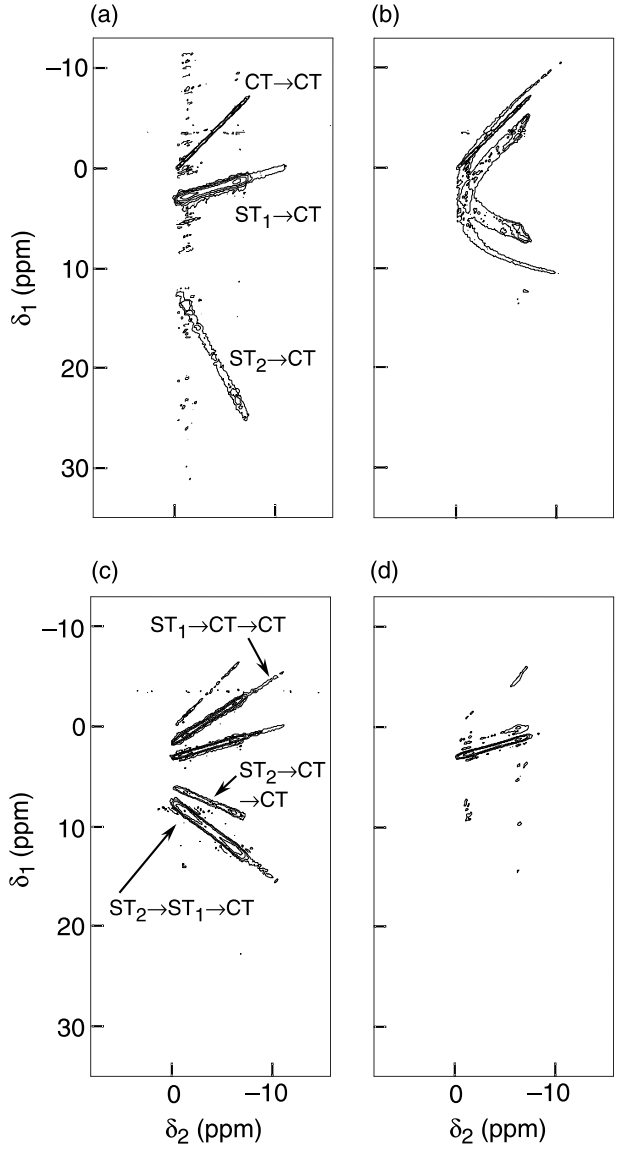

Fig. 4. ^{27}Al STMAS and SCAM-STMAS NMR of aluminium acetylacetonate, $Al(acac)_3$. (a,b) STMAS spectra recorded with the pulse sequence in Fig. 1a and (c,d) SCAM-STMAS spectra recorded with the pulse sequence in Fig. 1b. In (a,c) the magic angle was set as accurately as possible, while in (b,d) the magic angle was misset by ~0.09°. In (a,b) 32 and (c,d) 200 transients were averaged with a recycle interval of 1.0 s for each of 256 t_1 increments of 100 μs. The MAS rate was 20 kHz. All ppm scales are referenced to 1.0 M $Al(NO_3)_3$ (aq). Contour levels are shown at (a,c) 4, 8, 16, 32, and 64%, (b) 16, 32, 64%, and (d) 8, 16, 32, and 64% of the maximum intensity.

One of the goals of a two-dimensional STMAS experiment is to obtain the isotropic spectrum from a projection of the two-dimensional spectrum onto an axis orthogonal to the ridge lineshapes. Such an isotropic projection may be obtained through the use of a shearing transformation so that the lineshapes appear parallel to the F_2 (or δ_2) axis followed by a projection onto the F_1 (or δ_1) axis [19]. As an alternative to shearing, "split-t_1" experiments [21–24], with a t_1 period which is split between satellite- and central-transition evolution, may be employed [12,13]. The pulse sequence for a split-t_1 SCAM-STMAS experiment is shown in Fig. 1c. The position of the central-transition section of the t_1 evolution period, either before or after the final pulse, is dependent upon the sign of the STMAS ratio, whereas the values of k, k', and k'' are dependent upon the magnitude of this ratio. For example, for a spin $I = 5/2$ nucleus the $q = 3/2$ STMAS ratio is $R(5/2, 3/2) = +7/24$. The central-transition t_1 evolution, therefore, is placed after the final pulse, i.e., $k' = 0$. The values of $k = (1 + |R(I,q)|)^{-1}$ and k'' are given by 24/31 and 7/31, respectively (note that $k + k' + k'' = 1$).

Fig. 5 compares the signal intensities in isotropic ^{27}Al STMAS, SCAM-STMAS, and MQMAS NMR spectra of $Al(acac)_3$, obtained using split-t_1 shifted-echo experiments. The STMAS spectrum was recorded with the magic angle accurately set while the SCAM-STMAS and MQMAS spectra were recorded with an angle misset of ~0.09°. As with the central transition, the frequencies of symmetric ($m_I \leftrightarrow -m_I$) multiple-quantum transitions are always independent of the first-order quadrupolar interaction and MQMAS spectra, therefore, will not be affected by small deviations of the magic-angle setting. The intensities of the single isotropic peak in each spectrum are in the ratio 5.3:2.2:1.0 for STMAS, SCAM-STMAS and MQMAS, respectively. Although carefully optimised, the isotropic MQMAS spectrum in Fig. 5c was recorded without utilising any special methods to enhance sensitivity, such as RIACT, FAM, DFS, FASTER, and RAPT [6–9,25]. Despite much success having been achieved with these methods, it is notable that some of the most impressive relative signal enhancements have been attained for spin $I = 3/2$ nuclei, using only modest radiofrequency field strengths, and for solids where a good MQMAS signal-to-noise ratio is already available, thereby allowing easy optimisation.

Fig. 6a shows a two-dimensional ^{87}Rb STMAS spectrum of rubidium sulphate (Rb_2SO_4), recorded using a split-t_1 shifted-echo pulse sequence, with the magic

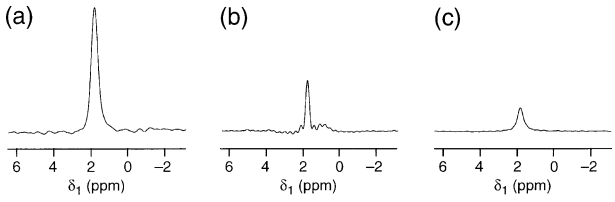

Fig. 5. Isotropic projections of (a) on-angle ^{27}Al STMAS, (b) off-angle ^{27}Al SCAM-STMAS and (c) off-angle ^{27}Al triple-quantum MAS spectra of $Al(acac)_3$. The relative intensities are absolute. All spectra were recorded with split-t_1 shifted-echo pulse sequences. The angle misset was ~0.09°. In (a) 192, (b) 200, and (c) 192 transients were averaged with a recycle interval of 1.0 s for each of 256 t_1 increments of 129.16 μs. The MAS rate was 20 kHz. All ppm scales are referenced to 1.0 M $Al(NO_3)_3$ (aq).

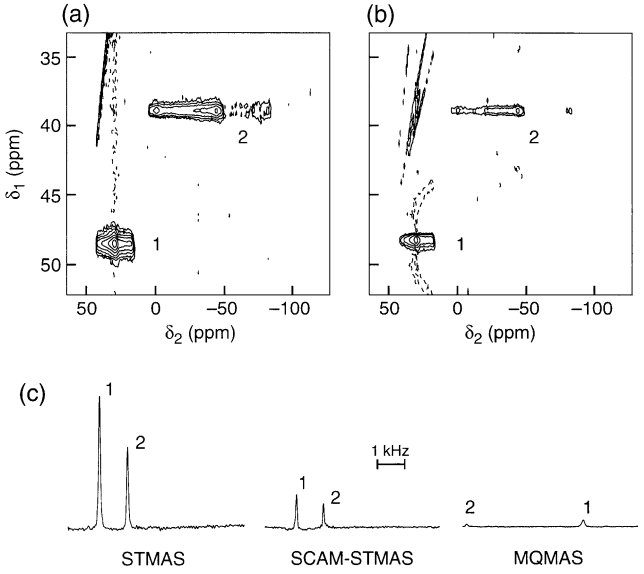

Fig. 6. ^{87}Rb STMAS and SCAM-STMAS NMR of rubidium sulphate, Rb_2SO_4. Two-dimensional (a) STMAS spectrum recorded with a split-t_1 pulse sequence and (b) SCAM-STMAS spectrum recorded with the split-t_1 pulse sequence in Fig. 1c. In (a) the magic angle was set as accurately as possible using our normal procedure, while in (b) the angle misset was ~0.09°. In (a) 96 and (b) 400 transients were averaged with a recycle interval of 0.5 s for each of (a) 300 and (b) 150 t_1 increments of (a) 62.96 μs and (b) 125.92 μs. The MAS rate was 30 kHz. All ppm scales are referenced to 1.0 M $RbNO_3$ (aq). Contour levels are shown at (a) 1, 2, 4, 8, 16, 32, and 64% and (b) 4, 8, 16, 32, and 64% of the maximum intensity. (c) Isotropic projections of split-t_1 STMAS, SCAM-STMAS and triple-quantum MAS NMR spectra. The peak amplitudes have been scaled in (c) to reflect the signal amplitude per unit experiment time. The peaks appear in different places in the isotropic STMAS and triple-quantum MAS spectra in (c) owing to (i) different chemical-shift scaling factors, x_{CS}, and (ii) aliasing.

angle set as accurately as possible using our normal procedure. There are expected to be two crystallographically distinct Rb nuclei in this material with ^{87}Rb C_Q values of 2.7 and 5.3 MHz [26] and two distinct lineshapes are observed in the spectrum. One lineshape is a short ridge parallel to the δ_2 axis, while the other, a much longer ridge, exhibits a very small but distinctive δ_1 splitting. The large quadrupolar interaction experienced by this ^{87}Rb nucleus results in an extreme sensitivity to any angle misset, making the setting of the angle with sufficient accuracy exceedingly difficult. The ^{87}Rb SCAM-STMAS spectrum of Rb_2SO_4, recorded using the pulse sequence in Fig. 1c, is shown in Fig. 6b. In this spectrum, recorded with an angle misset of ~0.09°, both ridge lineshapes are narrow and precisely parallel to the δ_2 axis. Here, as with the ^{27}Al results in Fig. 5, the SCAM-STMAS spectrum exhibits a signal intensity that is less than the STMAS spectrum but considerably greater than the corresponding triple-quantum MAS spectrum, with the three experiments yielding intensity ratios of 9.2:3.0:1.0 per unit measurement time, as shown by the isotropic projections in Fig. 6c. This particularly large sensitivity difference between SCAM-STMAS and MQMAS is probably a consequence of the fast MAS rate (30 kHz) required owing to the presence of large quadrupolar interactions (see below).

5. Linewidths in STMAS, SCAM-STMAS, and MQMAS spectra

The full linewidth at half-height in the isotropic ^{27}Al SCAM-STMAS spectrum of $Al(acac)_3$ in Fig. 5b (23 Hz) is significantly narrower than in the STMAS spectrum in Fig. 5a (44 Hz) despite the two experiments being recorded with the same maximum value of t_1. (Note that the SCAM-STMAS signal evens shows evidence of truncation in t_1.) This could be the result of a residual, but unavoidable, inaccuracy in the setting of the magic angle in the STMAS experiment. Interestingly, however, the SCAM-STMAS linewidth is also significantly narrower than the MQMAS linewidth in Fig. 5c (40 Hz). In order to gain an insight into the reason for the differing linewidths it is necessary to consider the possible mechanisms that may broaden these "isotropic" spectra.

In both STMAS and MQMAS experiments the quadrupolar interaction, first- and second-order in the case of STMAS and second-order only in the case of MQMAS, is removed from the isotropic spectrum by a combination of MAS and the correlation of two different transitions. Although it is known that other high-order interactions, including second-order quadrupolar–dipolar or quadrupolar–CSA cross-terms [27–32] and third-order quadrupolar effects [33], are not fully removed by MAS, in a large majority of cases these effects can be shown to be insignificant. (SCAM-STMAS experiments on solids where this is not the case are described in more detail below.) When measured in Hz, the isotropic shifts observed in high-resolution STMAS and MQMAS spectra are scaled relative to those found in a conventional MAS spectrum [13,34,35]. The chemical-shift scaling factors, $x_{CS}(I,q)$ and $x_{CS}(I,p)$ for STMAS and MQMAS, respectively, can be found in the literature [13,34]. Any inhomogeneous broadening present in the high-resolution spectrum, as a result of distributions of isotropic chemical shifts, distributions of quadrupolar parameters, or B_0 inhomogeneity, will be scaled by the corresponding x_{CS} factor [34]. This may result in linewidths that differ between various STMAS and MQMAS spectra: for example, it is almost certainly the explanation for much of the additional linewidth found in the isotropic ^{87}Rb MQMAS spectra in Fig. 6c compared with that in the STMAS and SCAM-STMAS spectra. However, the spin $I = 5/2$ scaling factors $x_{CS}(5/2, q = 3/2)$ and $x_{CS}(5/2, p = 3)$, for $q = 3/2$ STMAS and $p = 3$ MQMAS, respectively, are identical and so this cannot be the reason for the differing linewidths found in Fig. 5b and c.

It is known that MAS will remove all inhomogeneous broadening resulting from CSA or purely heteronuclear dipolar interactions, although any homogeneous broadening arising from strong homonuclear dipolar couplings is only removed when the MAS rate, ν_R, is much greater than the homogeneous static dipolar linewidth, $\Delta\nu_{stat}^{homo}$. Most quadrupolar nuclei have low or modest γ values and it seems likely that the condition $\nu_R \gg \Delta\nu_{stat}^{homo}$ holds in all cases considered in this work. In this strongly narrowed limit, homonuclear dipolar-driven spin diffusion will still oppose the narrowing effects of MAS and produce a residual homogeneous broadening [36,37]

$$\Delta\nu_{MAS}^{homo} \propto \frac{(\Delta\nu_{stat}^{homo})^2 k_{SD}}{\nu_{R^2}}, \quad (4)$$

where k_{SD} is the rate constant for spin diffusion across the static linewidth, itself probably proportional to $\Delta\nu_{stat}^{homo}$. The homogeneous static linewidth, $\Delta\nu_{stat}^{homo}$, is proportional to the coherence order $|p|$ and hence different between STMAS and MQMAS experiments. For example, $\Delta\nu_{stat}^{homo}$ in the triple-quantum dimension of an MQMAS experiment will be three times greater than in the corresponding dimension of an STMAS experiment. Owing to the $(\Delta\nu_{stat}^{homo})^2$ (or, possibly, $(\Delta\nu_{stat}^{homo})^3$ if $k_{SD} \propto \Delta\nu_{stat}^{homo}$) dependence of the residual broadening under MAS, it might then be expected that isotropic triple-quantum MAS spectra would display increased linewidths compared with isotropic SCAM-STMAS spectra, as observed in Fig. 5.

6. Effects of fast spinning

The signal intensity in an MQMAS experiment is known to decrease significantly as higher MAS rates, ν_R, are used [14]. In contrast, it has been shown that STMAS signal intensity remains almost invariant as the spinning rate changes [13]. Fig. 7 shows the effect of the MAS rate upon the amplitude of spin $I = 3/2$ SCAM ($ST^+ \rightarrow ST^-$) coherence transfer as a function of pulse duration. Simulations were performed for an on-resonance pulse with a radiofrequency field strength, ν_1, of 150 kHz and with $C_Q = 1.8$ MHz, $\eta = 0$ and $\nu_0 = 130$ MHz. The maximum coherence transfer amplitude decreases slightly as the spinning rate increases. For example, when $\nu_R = 30$ kHz the amplitude is only 90% of that obtained when $\nu_R = 10$ kHz. This behaviour is intermediate between that observed in STMAS and MQMAS. The excitation efficiencies in $I = 3/2$ STMAS ($I_z \rightarrow ST$) and MQMAS ($I_z \rightarrow 3Q$) when $\nu_R = 30$ kHz can be calculated to be 100 and 66%, respectively, of those obtained when $\nu_R = 10$ kHz [13]. The efficiency of the conversion pulses in STMAS ($ST \rightarrow CT$) and MQMAS ($3Q \rightarrow CT$) have both been shown to have similarly weak dependencies on the MAS rate [14]. It is expected, therefore, that the sensitivity of both STMAS and SCAM-STMAS will improve relative to MQMAS as higher spinning rates are used. Fig. 6c is probably an excellent example of this. Fast MAS rates are often required when large quadrupolar interactions are present (again, for example, as in Fig. 6) and these increase the difficulty of setting of the magic angle with sufficient accuracy, possibly making SCAM-STMAS the preferred method in these cases.

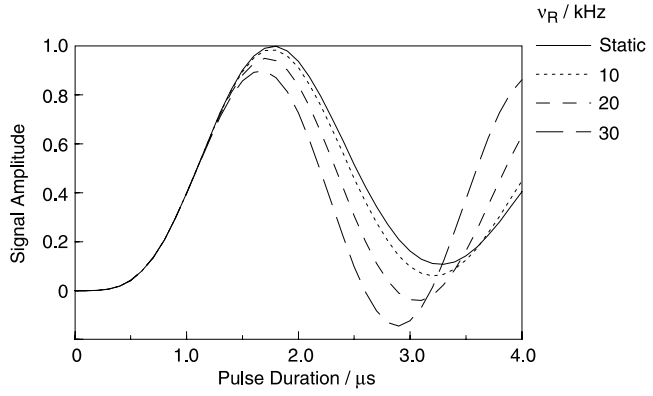

Fig. 7. The effect of MAS upon the amplitude of $I = 3/2$ SCAM ($ST^+ \rightarrow ST^-$) coherence transfer as a function of pulse duration. Simulations were performed for an on-resonance pulse with a radiofrequency field strength $\nu_1 = |\gamma B_1| = 150$ kHz and with $\nu_Q^{PAS} = 450$ kHz, $\eta = 0$, and $\nu_0 = 130$ MHz.

7. Tolerance of MAS rate instability

The rotor-synchronized acquisition employed in the t_1 dimension of STMAS experiments requires a stable spinning frequency, ν_R [1,2]. If the MAS rate drifts away from its desired value, even for a short period of time, the t_1 sampling will not be synchronized with the rotor and no STMAS signal will be obtained during this period. This will result in significant amounts of "t_1 noise" in the two-dimensional spectrum [38]. However, in many SCAM-STMAS spectra there appears to be a considerable reduction in the t_1 noise present, suggesting a increase in tolerance to these temporary spinning rate variations. An example is shown in Fig. 8a where two-dimensional ^{87}Rb STMAS and SCAM-STMAS spectra of $RbNO_3$ are compared, with low contour levels displayed. The STMAS spectrum displays a band of "noise", significantly larger than the true thermal noise and not appearing to be completely random, that runs parallel to the δ_1 axis wherever there is a strong resonance in the spectrum. This t_1 noise is therefore present in the isotropic STMAS projection shown in Fig. 8b. Note that this (and other projections in this work) is a true projection, with all signal intensity summed, not a so-called "skyline projection". However, the two dimensional SCAM-STMAS spectrum in Fig. 8a and its

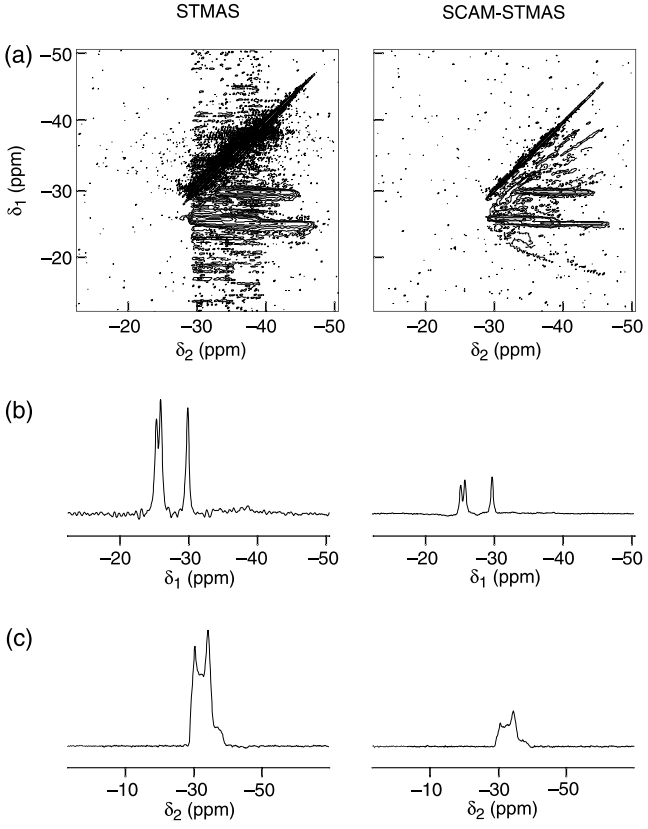

Fig. 8. ^{87}Rb STMAS and SCAM-STMAS NMR of rubidium nitrate, $RbNO_3$. (a) Two-dimensional on-angle STMAS and off-angle ($\sim$0.08°) SCAM-STMAS spectra recorded with split-t_1 pulse sequences, with (b) isotropic projections and (c) cross-sections parallel to the δ_2 axis at $\delta_1 = -26$ ppm. The relative intensities in (b) and (c) are absolute. For STMAS and SCAM-STMAS, respectively, 192 and 200 transients were averaged per t_1 increment with a recycle interval of 0.25 s. In each case, 128 t_1 increments of 188.89 μs were recorded. The MAS rate was 20 kHz. All ppm scales are referenced to 1.0 M $RbNO_3$ (aq). Contour levels are shown at 1, 2, 4, 8, 16, 32, and 64% and 4, 8, 16, 32, and 64% of the maximum intensity for the STMAS and SCAM-STMAS spectra, respectively.

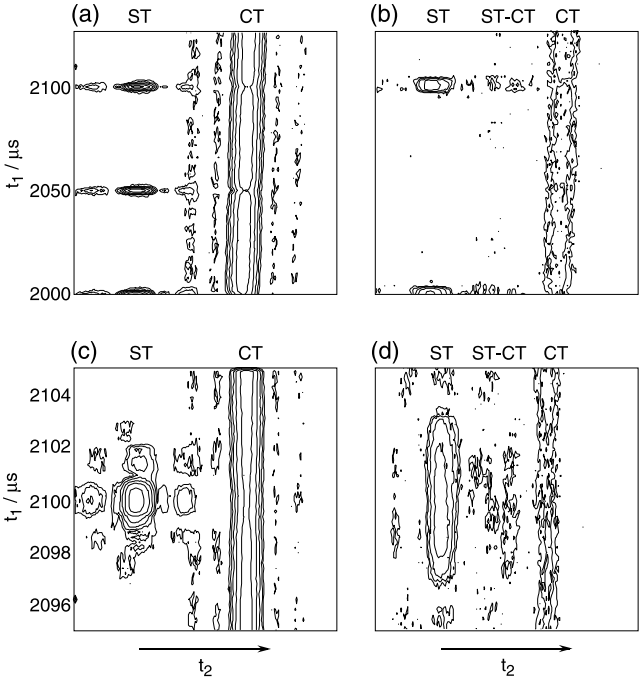

Fig. 9. Two-dimensional ^{87}Rb split-t_1 (a,c) STMAS and (b,d) SCAM-STMAS time-domain data sets (shown in magnitude mode) for $RbNO_3$. A t_1 increment much smaller than a rotor period was used to reveal the detailed structure of the satellite-transition rotational spin echoes. Coherence transfer echoes involving only satellite transitions in t_1 are labelled ST, those involving only central transitions are labelled CT, and those involving both satellite and central transitions in t_1 are labelled ST-CT.

isotropic projection in Fig. 8b show very little t_1 noise, with the lower contour levels in Fig. 8a revealing only a small amount of signal resulting from the unwanted $ST \rightarrow CT \rightarrow CT$ and $CT \rightarrow ST \rightarrow CT$ transfers. In contrast, Fig. 8c compares δ_2 cross-sections through one of the ^{87}Rb ridge lineshapes in both the STMAS and SCAM-STMAS spectra. The noise levels in both spectra are now identical as they result from true thermal noise only.

To demonstrate the origin of the increased tolerance to fluctuations in the MAS rate displayed by SCAM-STMAS, Fig. 9 shows (in magnitude mode) two-dimensional ^{87}Rb STMAS and SCAM-STMAS time-domain data sets for $RbNO_3$. These were recorded with increments of the t_1 evolution period that were much smaller than those needed for rotor synchronization and reveal the fine structure of the satellite-transition rotational spin echoes. In Fig. 9a, the STMAS time-domain data, two signals are observed; the $CT \rightarrow CT$ signal running throughout the t_1 acquisition, and the $ST \rightarrow CT$ signal appearing only when the t_1 period is equal to an integer number of rotor periods, i.e., when t_1 is rotor synchronized. In the SCAM-STMAS time-domain data in Fig. 9b, the $ST^{\pm} \rightarrow ST^{\mp} \rightarrow CT$ signal is observed only at even numbers of rotor periods. This is a consequence of the splitting of the t_1 period into two, with each half needing to be rotor synchronized for signal to be observed. The $CT \rightarrow CT \rightarrow CT$ signal is observed throughout the t_1 acquisition, while the signal resulting from $ST \rightarrow CT \rightarrow CT$ transfer is also observed but with low intensity. Figs. 9c and d show similar contour plots to those in Fig. 9a and b, expanded to show the area around a t_1 duration of 42 rotor periods (2100 μs). The STMAS time-domain data in Fig. 9c possess a maximum satellite-transition signal intensity when t_1 is exactly equal to 42 rotor periods, and significant signal intensity is only obtained when t_1 differs from this value by less than ± 0.5 μs. In contrast, the SCAM-STMAS time-domain data in Fig. 9d display significant satellite-transition signal intensity for $t_1 = 2100 \pm 2$ μs. This greater width of the SCAM-STMAS rotational spin echoes in the t_1 dimension is a consequence of the additional satellite-transition refocussing brought about by the SCAM pulse and explains the increased tolerance to

MAS rate fluctuations. It is easily seen that the effects of any mismatch between the t_1 sampling and the position of the rotational spin echoes will be less deleterious the broader those echoes are in the t_1 dimension.

8. Limits of angle-misset compensation

It has been shown above that SCAM-STMAS can refocus the first-order quadrupolar interaction introduced by a misset of the magic angle, but what are the limits to this angle-misset compensation? It can be seen from Eq. (3) that a misset of the angle χ will also affect the second-order quadrupolar shifts, although both the magnitude and sign of this interaction are the same for the two $q = 3/2$ satellite transitions. Therefore, a second-order quadrupolar broadening introduced by an angle misset into the high-resolution dimension cannot be refocussed in a SCAM-STMAS experiment. However, this effect is expected to be much smaller than the for first-order interaction considered previously. For example, the two spin $I = 3/2$ satellite transitions have a first-order splitting of $4\nu_Q^{\mathrm{PAS}} d^2_{0,0}(\chi) d^2_{0,0}(\beta)$ if $\eta = 0$. For a typical ν_Q^{PAS} value of 500 kHz this splitting will be of the order of 250 Hz if the magic angle is misset by $\pm 0.005°$. However, the second-order quadrupolar interaction is proportional to $(\nu_Q^{\mathrm{PAS}})^2/\nu_0$ and, assuming $\nu_0 = 100$ MHz, this same misset of the magic angle would result in an unwanted second-order broadening of $\lesssim 1$ Hz. The spinning angle would have to deviate from the magic angle by up to $\pm 1°$ to produce unwanted second-order broadenings of the order of 100 Hz.

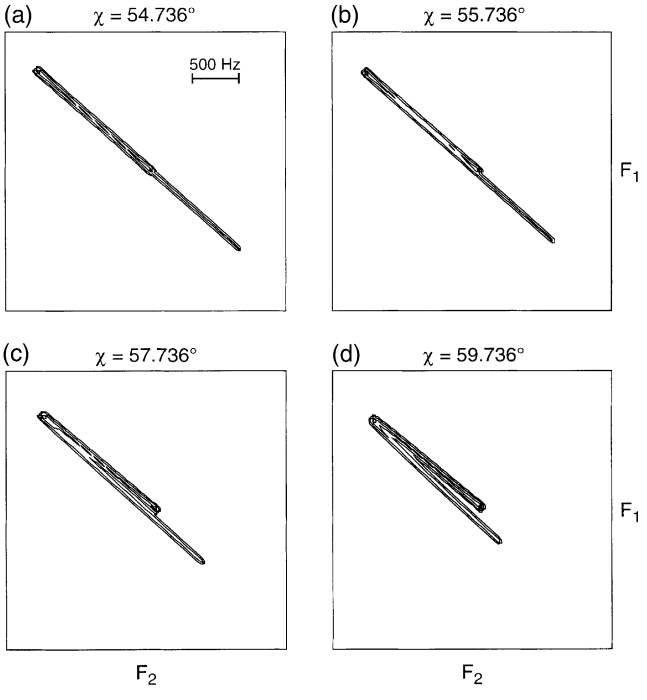

Fig. 10. Simulated two-dimensional $I = 3/2$ SCAM-STMAS spectra showing effects of severe spinning angle (χ) misset. The angle of the spinning axis χ is (a) 54.736° (the magic angle), (b) 55.736°, (c) 57.736°, and (d) 59.736°. Other parameters: $C_Q = 2$ MHz, $\eta = 0$, and $\nu_0 = 100$ MHz.

Fig. 10 shows spin $I = 3/2$ SCAM-STMAS spectra simulated using $C_Q = 2$ MHz, $\eta = 0$, $\nu_0 = 100$ MHz and χ values of 54.736° (the magic angle), 55.736°, 57.736°, and 59.736°, respectively. When the magic angle is correctly set, a narrow SCAM-STMAS ridge is observed lying along −8/9 (Fig. 10a). For an angle misset of +1° (Fig. 10b) all first-order splittings have been refocussed but a very small broadening of the ridge lineshape is observed as a result of the residual second-order quadrupolar interaction. As the angle misset is increased, the broadening of the ridge also increases and "isotropic" resolution is lost. When χ is misset by +5° (Fig. 10d) a broadening of several hundred hertz is observed. Of course, such significant deviations from the magic angle will also result in the reintroduction of dipolar and CSA interactions into SCAM-STMAS spectra and these, rather than the second-order quadrupolar interaction, are likely to be the limiting factors on isotropic resolution. Finally, it should be remembered that the MQMAS experiment will show similar sensitivity to these very large missets of the magic angle.

9. Alternative SCAM-STMAS experiments

9.1. SCAM-STMAS utilising $q = 5/2$ satellites

Nuclei with spin quantum number $I > 3/2$ possess more than one pair of satellite transitions, i.e., $q = 5/2$, 7/2, etc. For example, the ^{27}Al STMAS spectrum of $Al(acac)_3$ in Fig. 4a shows three ridges corresponding to $CT \rightarrow CT, ST_1 \rightarrow CT$, and $ST_2 \rightarrow CT$ transfer. It has been shown that the signal intensity in an STMAS spectrum decreases as the satellite-transition order q increases [13]. However, different STMAS experiments yield different chemical-shift scaling factors, $x_{CS}(I, q)$, and therefore may offer the possibility of increased resolution [13], depending upon the nature of the broadening mechanisms present [34]. As shown previously, the first-order quadrupolar interaction experienced by all pairs of satellite transitions is equal in magnitude but differs in sign. For example, for a spin $I = 5/2$ nucleus, such as ^{27}Al, the first-order quadrupolar shifts of the two satellite transitions are $\pm 2\nu_Q^{\mathrm{PAS}} d^2_{0,0}(\chi) d^2_{0,0}(\beta)$ and $\pm 4\nu_Q^{\mathrm{PAS}} d^2_{0,0}(\chi) d^2_{0,0}(\beta)$ for $q = 3/2$ and 5/2, respectively. In principle, therefore, SCAM-STMAS can be used to refocus the first-order quadrupolar interaction for any pair of satellite transitions, $ST_n^{\pm}$. Experimentally, the pulse duration required to obtain optimum $ST_n^+ \rightarrow ST_n^-$ transfer will be dependent upon the satellite-transition order.

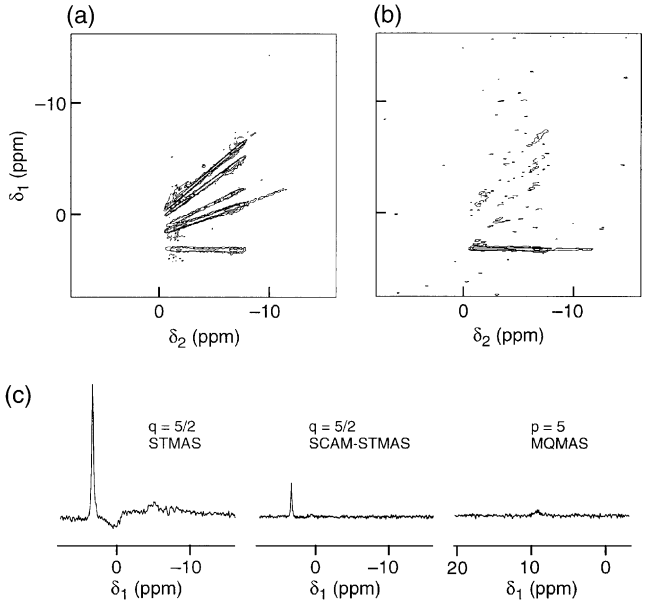

Fig. 11. ^{27}Al $q = 5/2$ STMAS and $p = 5$ MQMAS NMR of $Al(acac)_3$. (a) On-angle two-dimensional SCAM-STMAS spectrum recorded with the split-t_1 pulse sequence in Fig. 1c. (b) Corresponding off-angle (~0.07°) spectrum. In each case, 200 transients were averaged with a recycle interval of 1.0 s for each of 184 t_1 increments of 283.33 μs. The MAS rate was 20 kHz. All ppm scales are referenced to 1.0 M $Al(NO_3)_3$ (aq). Contour levels are shown at (a) 8, 16, 32, and 64% and (b) 10, 20, 40, and 80% of the maximum intensity. (c) Isotropic projections of split-t_1 $q = 5/2$ STMAS, $q = 5/2$ SCAM-STMAS and $p = 5$ MQMAS NMR spectra. The peak amplitudes have been scaled in (c) to reflect the signal amplitude per unit experiment time. Owing to the different chemical-shift scaling factors between the $q = 5/2$ STMAS and $p = 5$ MQMAS experiments the peaks in (c) have different δ_1 shifts.

Fig. 11a shows the two-dimensional ^{27}Al SCAM-STMAS spectra of $Al(acac)_3$ recorded using the split-t_1 pulse sequence shown in Fig. 1c, with $k = (1 + |R(5/2, 5/2)|)^{-1}$ and an accurately set magic angle. All pulse durations have been experimentally optimized for transfers involving the $q = 5/2$, or ST_2, satellite transitions. A narrow ridge lying parallel to the δ_2 axis is observed, corresponding to the single crystallographically distinct Al site. The other ridges, lying along different gradients, result from mixed transfer pathways involving the CT, ST_1 and ST_2 transitions. When the magic angle is misset by ~0.07°, as shown in Fig. 11b, these unwanted ridges experience a large first-order quadrupolar interaction and are unobservable. However, SCAM-STMAS has refocussed the angle misset through $ST_2^{\pm} \rightarrow ST_2^{\mp} \rightarrow CT$ transfer, yielding a single narrow ridge parallel to δ_2. Although, the intensity of the $q = 5/2$ SCAM-STMAS spectrum is only 25% of that obtained using a $q = 5/2$ STMAS experiment, as shown in Fig. 11c, the linewidth is considerably narrower and the t_1 noise considerably less. Both experiments yield less signal intensity than the corresponding $q = 3/2$ STMAS experiment and, moreover, the $q = 5/2$ SCAM-STMAS spectrum possesses less signal than a triple-quantum MAS spectrum (not shown). However, both $q = 5/2$ STMAS and $q = 5/2$ SCAM-STMAS display considerably more signal intensity than the five-quantum MAS spectrum, also shown in Fig. 11c. The $q = 5/2$ SCAM-STMAS spectrum displays the narrowest linewidth of the three projections in Fig. 11c, with a full-width at half-height of 18 Hz, compared with 30 Hz and ~90 Hz for the $q = 5/2$ STMAS and $p = 5$ MQMAS spectra, respectively. Again, it should be noted that, although the chemical-shift scaling factor for an $I = 5/2$ five-quantum MAS experiment ($x_{CS}(5/2, 5) = 85/37$) is larger than that for a $q = 5/2$ STMAS experiment ($x_{CS}(5/2, 5/2) = +1$), this cannot fully explain the relatively large linewidth found in the five-quantum MAS experiment.

9.2. Self-compensated double-quantum satellite-transition MAS

All the SCAM-STMAS experiments described above achieve refocussing of the angle misset through correlation of single-quantum ST_n^+ and ST_n^- coherences

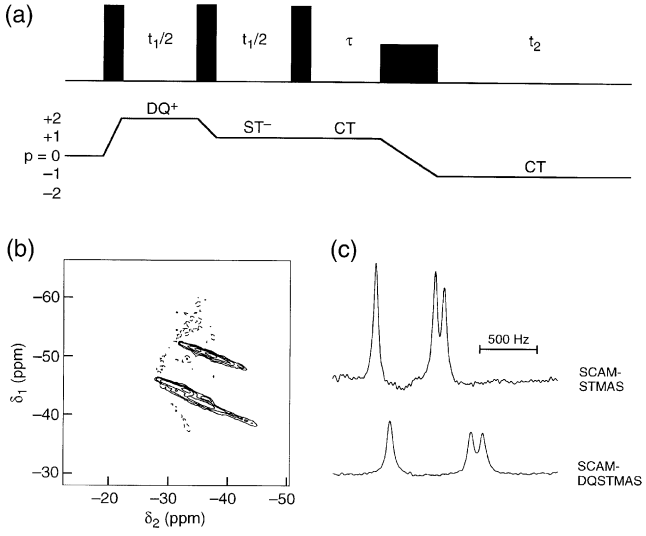

Fig. 12. (a) Pulse sequence and coherence transfer pathway for a shifted-echo SCAM-DQSTMAS experiment. A 160-step phase cycle can be used to select the desired coherence pathways: first pulse, 0° 45° 90° 135° 180° 225° 270° 315°; second pulse, 0°; third pulse, 32(0°) 32(72°) 32(144°) 32(216°) 32(288°); fourth pulse, 8(0°) 8(90°) 8(180°) 8(270°); receiver, 2(0° 270° 180° 90°) 2(180° 90° 0° 270°). (b) Two-dimensional ^{87}Rb SCAM-DQSTMAS spectrum of $RbNO_3$ recorded with the pulse sequence in (a) with an angle misset of ~0.08°. Eight hundred transients were averaged with a recycle interval of 0.25 s for each of 128 t_1 increments of 100 μs. The MAS rate was 20 kHz. All ppm scales are referenced relative to 1.0 M $RbNO_3$ (aq). Contour levels are shown at 8, 16, 32, and 64% of the maximum intensity. (c) Isotropic projections of ^{87}Rb SCAM-STMAS and SCAM-DQSTMAS spectra, recorded with split-t_1 pulse sequences. The peak amplitudes in these projections have been scaled to reflect the signal amplitude per unit experiment time.

during the t_1 period. It is also possible to refocus an angle misset through correlation of single-quantum satellite transitions with any other transitions that possess a first-order quadrupolar broadening, such as double-quantum coherences. Fig. 12a shows a pulse sequence and coherence transfer pathway diagram for a double-quantum (DQ) STMAS experiment that self-compensates for angle misset. An initial pulse creates double-quantum coherences which evolve for a period $t_1/2$, after which they are converted to single-quantum satellite-transition coherences for the remainder of the t_1 period. Although the second-order shifts are different, the two inner double-quantum satellite transitions (DQ_1^+ with $m_I = +3/2 \leftrightarrow -1/2$ and DQ_1^- with $m_I = +1/2 \leftrightarrow -3/2$) exhibit first-order quadrupolar shifts that are identical to those of the two $q = 3/2$ satellite transitions.

A two-dimensional ^{87}Rb SCAM-DQSTMAS spectra of $RbNO_3$, recorded with the pulse sequence in Fig. 12a and with χ misset by $\sim 0.08°$, is shown in Fig. 12b. Three ridge lineshapes, corresponding to the three distinct Rb sites, are observed lying along the predicted gradient of $-7/18$, showing that the splitting arising from the angle misset has been refocussed. The use of double-quantum coherences is expected to result in a significant decrease in signal intensity, however. Fig. 12c shows isotropic projections of both ^{87}Rb SCAM-STMAS and self-compensated double-quantum satellite-transition MAS (SCAM-DQSTMAS) spectra of $RbNO_3$ with the latter exhibiting only $\sim 35\%$ of the intensity observed in the former. We would expect that any of the many other possible multiple-quantum satellite-transition experiments providing angle-misset compensation would also yield similarly reduced sensitivity.

10. Refocussing of other high-order interactions

It has recently been shown that lineshapes in MQMAS spectra may exhibit splittings or broadenings if there is dipolar coupling to another quadrupolar nucleus [27–32]. This quadrupolar–dipolar cross-term interaction limits the spectral resolution as it is second order in nature and, therefore, not removed fully by MAS. Similar high-order effects, such as quadrupolar–dipolar and quadrupolar–CSA cross-term interactions, are present in STMAS spectra [12,27,32]. More recently, the presence of third-order quadrupolar effects in STMAS spectra has been demonstrated [33]. The effect of some of these high-order interactions upon SCAM-STMAS spectra are now considered.

10.1. Third-order quadrupolar effects

When the quadrupolar interaction is very large a third-order approximation may be required to describe the system. Third-order quadrupolar effects are proportional to $(\nu_Q^{PAS})^3/\nu_0^2$, increasing rapidly, therefore, with increasing ν_Q^{PAS} or with decreasing Larmor frequency [33]. The third-order quadrupolar interaction is expected to consist of zero-, second-, fourth- and sixth-rank terms, and consequently will not be removed fully by MAS [33]. As with the first-order interaction, the third-order quadrupolar interaction does not perturb central or symmetric multiple-quantum transition frequencies and so will not affect MQMAS spectra. However, a third-order splitting is present in the satellite transitions and is predicted to affect STMAS spectra, ultimately limiting the achievable spectral resolution. Although any third-order shifts will be much smaller than the first- and second-order quadrupolar shifts, they may be observable in the isotropic dimension of an STMAS spectrum where both the first- and second-order interactions are fully suppressed (provided the magic angle is accurately set).

Fig. 13 shows two-dimensional ^{27}Al split-t_1 STMAS and SCAM-STMAS spectra of andalusite (Al_2SiO_5), an aluminosilicate mineral. Two distinct ^{27}Al resonances are expected in andalusite, with C_Q values of 5.6 and 15.3 MHz, respectively [39]. The STMAS spectrum in Fig. 13a displays two ^{27}Al ridge lineshapes and both possess a considerable δ_1 splitting indicating that there is a misset of the magic angle (estimated to be $-0.03°$). As the spinning angle χ is gradually increased by manual adjustment of the NMR probehead, the δ_1 splitting of the Al site with the smaller C_Q value decreases until, as shown in Fig. 13b, a narrow ridge is obtained for this site. Further increase in the spinning angle reintroduces an δ_1 splitting into this resonance, hence we can assume that a magic-angle misset (estimated to be $+0.02°$) is now present again. However, the behaviour of the broader lineshape in Figs. 13a–c is much more complex, with very different lineshapes observed in the three spectra. A considerable δ_1 splitting is always observed, even when the magic angle is apparently set accurately, as in Fig. 13b [33]. It has been suggested that this splitting arises from a third-order quadrupolar effect resulting from the large quadrupolar interaction, $\nu_Q^{PAS} = 1.15$ MHz [33]. The effect is surprisingly large, of the order of 1 kHz, but still considerably smaller than the second-order quadrupolar broadening of ~ 30 kHz. It should also be noted that the spectra recorded with a spinning angle χ below and above $54.736°$ exhibit significantly different lineshapes. If this is indeed a third-order quadrupolar interaction, it is interesting to note that there must be a strong dependence upon the spin quantum number I [32,33]. One of the two distinct spin $I = 3/2$ ^{87}Rb nuclei in Rb_2SO_4 possesses a C_Q value of 5.3 MHz [26], corresponding to a ν_Q^{PAS} value of 1.33 MHz, considerably larger than that found in andalusite. However, a much smaller splitting, less than 40 Hz, was observed in the ^{87}Rb STMAS spectrum in Fig. 6a when the magic angle was set as accurately as possible.

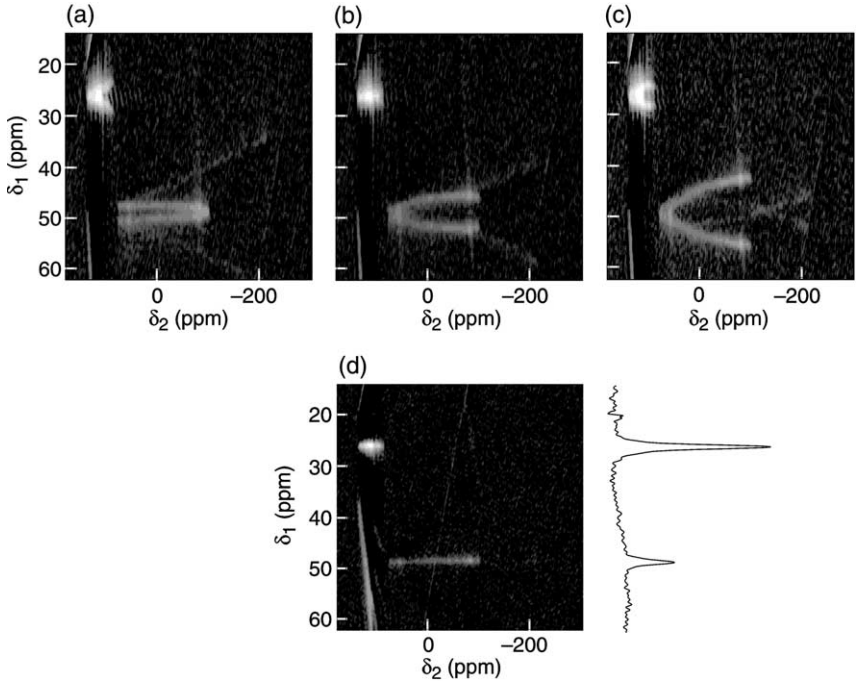

Fig. 13. ^{27}Al STMAS and SCAM-STMAS NMR of andalusite, Al_2SiO_5. (a–c) Two-dimensional STMAS spectra recorded with a split-t_1 pulse sequence. The spinning angle was varied such that it appears to be set to the magic angle in (b) and either side of it in (a) and (c). (d) Two-dimensional SCAM-STMAS spectrum and isotropic projection, recorded using the pulse sequence in Fig. 1b with an angle misset of ~0.07°. In (a-c) 288 transients were averaged with a recycle interval of 0.5 s for each of 230 t_1 increments of 43.02 μs. In (d) 1600 transients were averaged with a recycle interval of 0.5 s for each of 192 t_1 increments of 86.04 μs. The MAS rate was 30 kHz. All ppm scales are referenced to 1.0 M $Al(NO_3)_3$ (aq).

It can be seen from Fig. 13b that the two $q = 3/2$ satellite transitions exhibit third-order quadrupolar shifts which are equal in magnitude but opposite in sign. As with a first-order quadrupolar interaction, therefore, SCAM-STMAS should refocus the splitting and produce a high-resolution spectrum. Fig. 13d shows a two-dimensional ^{27}Al SCAM-STMAS spectrum of andalusite, recorded using the pulse sequence in Fig. 1c, with an angle misset of ~0.07°. Two ridge lineshapes lying parallel to the δ_2 axis are observed and the high-resolution spectrum consists of two narrow resonances. Therefore, the resolution of a SCAM-STMAS spectrum is not limited by the presence of these third-order quadrupolar effects.

10.2. Quadrupolar–CSA cross-term interactions

We have recently demonstrated that STMAS spectra are affected by the presence of a cross-term interaction between the quadrupolar and CSA interactions [32]. Typically, this cross-term interaction is small, but for nuclei with very large CSA interactions, such as ^{59}Co ($I = 7/2$), significant F_1 splittings may be observed. The central and symmetric multiple-quantum transitions remain unaffected by this interaction and so similar splittings are not found in MQMAS spectra. Fig. 14a shows a ^{59}Co STMAS spectrum of cobalt acetylacetonate, $Co(acac)_3$, recorded using the pulse sequence

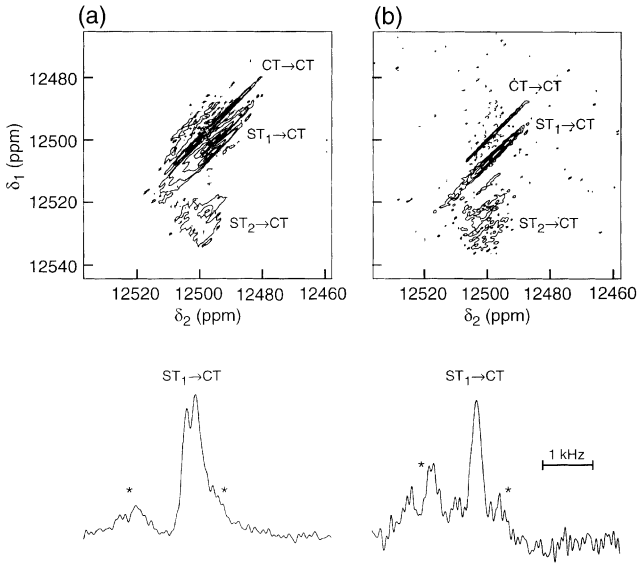

Fig. 14. ^{59}Co STMAS and SCAM-STMAS NMR of cobalt acetylacetonate, $Co(acac)_3$. Two-dimensional (a) on-angle STMAS and (b) off-angle (~0.08°) SCAM-STMAS spectra and corresponding isotropic projections, recorded using the pulse sequences in Figs. 1a and b, respectively. In (a) 640 and (b) 3200 transients were averaged with a recycle interval of 1.0 s for each of (a) 128 and (b) 80 t_1 increments of (a) 50 and (b) 100 μs. The MAS rate was 20 kHz. The asterisks in the projections indicate signal intensity from CT → CT and ST_2 → CT peaks. All ppm scales are referenced to 1.0 M $K_3[Co(CN)_6]$ (aq). Contour levels are shown at (a) 6, 12, 22, 32, 52, 72, and 92% and (b) 12, 22, 32, 52, 72, and 92% of the maximum intensity.

shown in Fig. 1a. Although the magic angle is accurately set (determined from ^{87}Rb STMAS experiments on $RbNO_3$, recorded both prior and subsequent to this spectrum), the $ST_1 \rightarrow CT$ peak displays a splitting of $\sim$200 Hz in the isotropic projection as a result of a quadrupolar–CSA cross-term interaction [32]. The other peaks observed in the two-dimensional spectrum originate from $CT \rightarrow CT$ and $ST_2 \rightarrow CT$ correlations. A third-order quadrupolar splitting can be ruled out in this case as the quadrupolar interaction is small ($\nu_Q^{PAS} =$ 200 kHz), while the CSA is large ($\delta_{CSA} = 700$ ppm). Fig. 14b displays the corresponding SCAM-STMAS spectrum recorded using the pulse sequence in Fig. 1b with an angle misset of $\sim$0.08°. Despite the significant misset of the magic angle, a single ridge is observed arising from the $ST_1^{\pm} \rightarrow ST_1^{\mp} \rightarrow CT$ coherence transfer that refocuses both the angle misset and the splitting arising from the quadrupolar–CSA cross-term.

11. Improved coherence transfer efficiency (FAM-SCAM)

The difference in sensitivity between the STMAS and SCAM-STMAS experiments demonstrated in this work is a consequence of the relative inefficiency of $ST^{\pm} \rightarrow ST^{\mp}$ coherence transfer by the second pulse of the sequence in Fig. 1b. An important developmental aim, therefore, is to increase the efficiency of this transfer. Amplitude-modulated composite pulses, which in this application are often termed fast-amplitude-modulated (FAM) pulses [7], have been used to enhance triple- to single-quantum transfer in MQMAS experiments by factors of up to 2 or 3. Pulses of the form $\{\beta_x - \tau - \beta_{-x} - \tau -\}_n$ and $\beta_x\beta'_{-x}\beta''_x \cdots$ have been employed for spin $I = 3/2$ and $I = 5/2$ experiments, respectively, often with the largest enhancements observed in the former case. We have employed a mixture of computer minimization and experimental optimisation of FAM-SCAM pulses of the form $\beta_x\beta'_{-x}\beta''_x \cdots$ to enhance SCAM-STMAS transfer.

Fig. 15a shows two-dimensional off-angle ($\sim$0.08°) ^{87}Rb SCAM-STMAS NMR spectra of $RbNO_3$, recorded with the pulse sequence in Fig. 1c. In the FAM-SCAM version, the second pulse has been replaced with a $(1.8\,\mu s)_x\ (1.8\,\mu s)_{-x}$ composite pulse which enhances the sensitivity of the experiment by an average of $\sim$25%, as shown in the isotropic projections in Fig. 15b. Note also, in Figs. 15a and b, that the FAM-SCAM pulse appears to have reduced the intensity of some of the unwanted correlations occurring in SCAM-STMAS. Similar results are obtained at a slower MAS rate of 10 kHz, with the enhancement here closer to an average of $\sim$50%, as shown in Fig. 15c. These results, although only preliminary, suggest that there is considerable scope for reducing the sensitivity gap between SCAM-STMAS and STMAS.

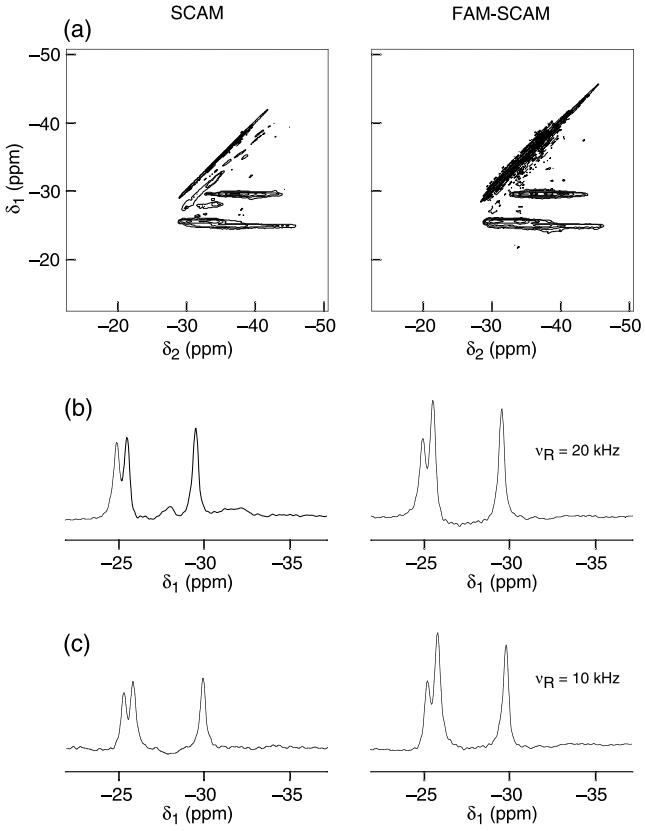

Fig. 15. ^{87}Rb SCAM-STMAS NMR of $RbNO_3$. (a) Two-dimensional off-angle ($\sim$0.08°) SCAM-STMAS spectra recorded with the split-t_1 pulse sequence in Fig. 1c. In the FAM-SCAM version an experimentally optimised $(1.8\,\mu s)_x\ (1.8\,\mu s)_{-x}$ pulse was used in place of the simple 1.4 μs SCAM pulse to enhance the sensitivity. For each spectrum, 400 transients were averaged with a recycle interval of 0.25 s for each of 128 t_1 increments of 188.9 μs. The MAS rate was 20 kHz. All ppm scales are referenced to 1.0 M $RbNO_3$ (aq). Contour levels are shown at (a) 8, 16, 32, and 64% and (b) 4, 8, 16, 32, and 64% of the maximum intensity. (b) Isotropic projections of the two-dimensional SCAM-STMAS spectra in (a). (c) Isotropic SCAM-STMAS spectra recorded with a MAS rate of 10 kHz and with 200 transients averaged with a recycle interval of 0.25 s for each of 64 t_1 increments of 377.7 μs. A $(2.0\,\mu s)_x\ (2.0\,\mu s)_{-x}$ experimentally optimised FAM-SCAM pulse was used.

12. Conclusions

The major limitation to the implementation of STMAS has been the required accuracy of the magic-angle setting, with an accuracy of close to ±0.001° often needed. Here, we have described a variant of the STMAS experiment (SCAM-STMAS) that self-compensates for angle missets of up to ±1°. The technique has been successfully demonstrated on a variety of $I = 3/2$, 5/2, and 7/2 systems with differing quadrupolar interactions. We envisage the main uses of this technique to be: (i) in materials with large quadrupolar interactions where accurate setting of the magic angle is practically difficult and where MQMAS suffers from a severe lack of sensitivity owing to the poor coherence transfer

efficiencies and fast MAS rates required and (ii) on NMR probeheads whose design makes very accurate calibration and retention of the magic angle difficult.

It has been shown that SCAM-STMAS has a lower sensitivity than STMAS but preliminary results using composite pulses have yielded sensitivity enhancements of between 25 and 50% and offer great promise for future work. The sensitivity of SCAM-STMAS was found to be higher than that of MQMAS in all cases considered here (i.e., Figs. 5 and 6) and in [15]. The resolution of SCAM-STMAS has been demonstrated to be consistently higher than that of STMAS, as might perhaps be expected, but has also been shown in some cases to be significantly higher than that of MQMAS. One possible explanation considered here lies in the nature of the residual homogeneous dipolar broadening under MAS. The SCAM-STMAS experiment has also been shown to display an increased tolerance of MAS rate fluctuations, resulting in a significant reduction in the t_1 noise present in the two-dimensional spectrum.

In addition to SCAM-STMAS experiments involving only the $q = 3/2$ or ST_1 satellite transitions, we have successfully demonstrated SCAM-STMAS experiment utilising the $q = 5/2$ or ST_2 transitions in a spin $I = 5/2$ experiment. Angle-misset compensated STMAS experiments involving double-quantum coherences have also been demonstrated but, although easy to implement, display reduced sensitivity owing to the inefficiency of double-quantum excitation and conversion. Finally, we have shown that the resolution of SCAM-STMAS experiments is not limited by the presence of other high-order effects that can broaden satellite transitions, such as quadrupolar–CSA cross-term or third-order quadrupolar interactions.

Acknowledgments

We are grateful to EPSRC for generous support (Grant No. GR/N07622) and to Professor Peter W. Scott (Camborne School of Mines, University of Exeter, UK) for the andalusite sample.

References

[1] Z. Gan, J. Am. Chem. Soc. 122 (2000) 3242.
[2] Z. Gan, J. Chem. Phys. 114 (2001) 10845.
[3] L. Frydman, J.S. Harwood, J. Am. Chem. Soc. 117 (1995) 5367.
[4] S. Ganapathy, S. Schramm, E. Oldfield, J. Chem. Phys. 77 (1982) 4360.
[5] J.P. Amoureux, Solid State Nucl. Magn. Reson. 2 (1993) 83.
[6] G. Wu, D. Rovnyak, R.G. Griffin, J. Am. Chem. Soc. 118 (1996) 9326.
[7] P.K. Madhu, A. Goldburt, L. Frydman, S. Vega, Chem. Phys. Lett. 307 (1999) 41.
[8] A.P.M. Kentgens, R. Verhagen, Chem. Phys. Lett. 300 (1999) 435.
[9] T. Vosegaard, P. Florian, D. Massiot, P.J. Grandinetti, J. Chem. Phys. 114 (2001) 4618.
[10] J.P. Amoureux, C. Fernandez, L. Frydman, Chem. Phys. Lett. 259 (1996) 347.
[11] J.P. Amoureux, C. Fernandez, Solid State Nucl. Magn. Reson. 10 (1998) 211.
[12] K.J. Pike, S.E. Ashbrook, S. Wimperis, Chem. Phys. Lett. 345 (2001) 400.
[13] S.E. Ashbrook, S. Wimperis, J. Magn. Reson. 156 (2002) 269.
[14] J.P. Amoureux, M. Pruski, D.P. Lang, C. Fernandez, J. Magn. Reson. 131 (1998) 170.
[15] S.E. Ashbrook, S. Wimperis, J. Am. Chem. Soc. 124 (2002) 11602.
[16] R.N. Zare, Angular Momentum, Wiley, Chichester, 1996.
[17] P.J. Grandinetti, J.H. Baltisberger, A. Llor, Y.K. Lee, U. Werner, M.A. Eastman, A. Pines, J. Magn. Reson. A 103 (1993) 72.
[18] D. Massiot, B. Touzo, D. Trumeau, J.P. Coutures, J. Virlet, P. Florian, P.J. Grandinetti, Solid State Nucl. Magn. Reson. 6 (1996) 73.
[19] R.R. Ernst, G. Bodenhausen, A. Wokaun, Principles of Nuclear Magnetic Resonance in One and Two Dimensions, Clarendon Press, Oxford, 1987.
[20] C. Huguenard, F. Taulelle, B. Knott, Z. Gan, J. Magn. Reson. 156 (2002) 131.
[21] S.P. Brown, S.J. Heyes, S. Wimperis, J. Magn. Reson. A 119 (1996) 280.
[22] S.P. Brown, S. Wimperis, J. Magn. Reson. 124 (1997) 279.
[23] S.P. Brown, S. Wimperis, J. Magn. Reson. 128 (1997) 42.
[24] S.P. Brown, S.E. Ashbrook, S. Wimperis, J. Phys. Chem. B 103 (1999) 812.
[25] H.-T. Kwak, S. Prasad, Z. Yao, P.J. Grandinetti, J.R. Sachleben, L. Emsley, J. Magn. Reson. 150 (2001) 71.
[26] J.H. Baltisberger, S.L. Gann, E.W. Wooten, T.H. Chang, K.T. Mueller, A. Pines, J. Am. Chem. Soc. 114 (1992) 7489.
[27] G. Wu, R.E. Wasylishen, Mol. Phys. 95 (1998) 1177.
[28] G. Wu, K. Yamada, Chem. Phys. Lett. 313 (1999) 519.
[29] J. McManus, R. Kemp-Harper, S. Wimperis, Chem. Phys. Lett. 311 (1999) 292.
[30] S. Wi, L. Frydman, J. Chem. Phys. 112 (2000) 3248.
[31] S. Wi, V. Frydman, L. Frydman, J. Chem. Phys. 114 (2001) 8511.
[32] S. Wi, S.E. Ashbrook, S. Wimperis, L. Frydman, J. Chem. Phys. 118 (2003) 3131.
[33] Z. Gan, P. Srinivasan, J.R. Quine, S. Steuernagel, B. Knott, Chem. Phys. Lett. 367 (2003) 163.
[34] K.J. Pike, R.P. Malde, S.E. Ashbrook, J. McManus, S. Wimperis, Solid State Nucl. Magn. Reson. 16 (2000) 203.
[35] J.P. Amoureux, C. Huguenard, F. Engelke, F. Taulelle, Chem. Phys. Lett. 356 (2002) 497.
[36] M.M. Maricq, J.S. Waugh, J. Chem. Phys. 70 (1979) 3300.
[37] S.E. Ashbrook, S. Antonijevic, A.J. Berry, S. Wimperis, Chem. Phys. Lett. 364 (2002) 634.
[38] A.F. Mehlkopf, D. Korbee, T.A. Tiggleman, R. Freeman, J. Magn. Reson. 58 (1984) 315.
[39] L.B. Alemany, S. Steuernagel, J.P. Amoureux, R.L. Callender, A.R. Barron, Solid State Nucl. Magn. Reson. 14 (1999) 1.